Proceedings of the 1998 IEEE/RSJ
Intl. Conference on Intelligent Robots and Systems
Victoria, B.C., Canada • October 1998

Design and Analysis of a Parallel-Type Gripping and Micro-Positioning Mechanism

B.-J. Yi[1], K.H Cho[1], J.H. Lee[1], S.-R. Oh[2], I.H. Suh[3], W.K. Kim[4]

[1]Dept. of Control and Instrumentation Eng., Hanyang Univ. Korea
[2]Div. of Electronics and Information Tech., KIST, Korea
[3]Dept. of Electronics Eng., Hanyang Univ. Korea
[4]Dept. of Control and Instrumentation Eng., Korea Univ. Korea

Abstract

In this work, a parallel-type gripping and micro-positioning mechanism is proposed. This device has a parallelogramic platform which can be flexibly folded. Therefore, this mechanism not only can be used to grasp an object having irregular shape or large volume, but also can be utilized as a micro-positioning device after grasping the object. Configuration parameter for configuration control of the proposed gripping mechanism is defined. Grasping force and isotropic characteristic of the mechanism are considered as design indices for optimal design of the gripping mechanism. The proposed mechanism is expected to be used as an adaptable gripping and micro-positioning device by attaching it at the end-point of a robot.

1. Introduction

Investigation on controlling the shape of robot configuration utilizing the kinematic redundancies has been called "configuration control". However, studies on such subject have been confined to kinematically redundant serial manipulators[1-2], but study on configuration control for parallel manipulator has been rare while studies on parallel manipulators have been progressed recently[3-16]. In this study, we discuss configuration control using a parallel-type gripping manipulator. Consider two different parallel manipulators given in Fig. 1 and Fig. 2. The parallel manipulator of Fig. 1 has a rigid platform, while the parallel manipulator of Fig. 2 has a nonrigid platform since the links on the platform are connected by joints. A conceptual schematic for this mechanism is shown in Fig. 3. Note that two revolute joints exist at each vertice of the platform. Therefore, the shape of the platform can be changed.

Mobility is defined as *the number of independent variables which must be specified in order to locate its elements relative to another.* It is described by [3]

$$M = N(L-1) - \sum_{i=1}^{J}(N-F_i), \qquad (1)$$

where N, L, J, and F_i denote the degree-of-freedom of the operational (or task) space, the number of links, the number of joints, and the motion degree-of-freedom of the *ith* joint, respectively. Mobility also represents the minimum number of the system actuator. When M is greater than N, the system is called *a kinematically redundant system*. The mobility of the parallel manipulator shown in Fig. 1 is 3, and thus it can control 3 degrees of motion in the operation space(i.e., the motion in the x- and y-directions, and the rotation angle of the platform). In the literature, only a planar parallel mechanism having only three-chains has been considered. The four-closed chain parallel mechanism has better stiffness and load handling capacity via additional base actuation, as compared to the three-closed chain system. In the meanwhile, the mobility of the parallel manipulator shown in Fig. 2 (or Fig. 3) is 4, and thus it can control the same 3 directional motions in the operation space along with one other parameter. Consider this additional parameter as the shape of the platform. We expect that this parallel system can be utilized as a gripper mechanism by shaping the platform configuration. Currently employed robot gripper has a simple geometry which is often not appropriate to grasp an object having irregular shape or large volume. On the other hand, the proposed gripper mechanism is expected to be able to grasp any object having irregular shape or large volume and also it can be utilized as a micro-positioning device after grasping. Figure 4 shows a 3 DOF parallel manipulator which consists of several links and joints. Since the triangular-shaped platform always maintains its

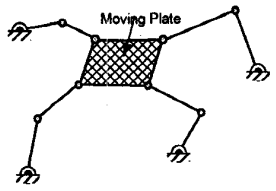

Figure 1. Parallel manipulator with mobility 3

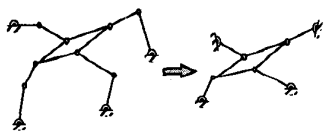

Figure 2. Parallel manipulator with mobility 4

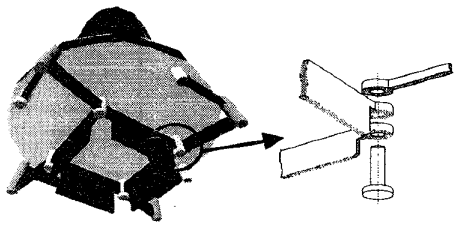

Figure 3. Conceptual Schematic of the Gripping Mechanism

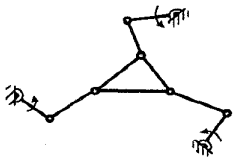

Figure 4. Parallel manipulator with mobility 3 (Configuration uncontrollable)

shape whether the platform is a rigid body or not, the shape of the platform system cannot be configured. Even for the case of Figure 2, success of configuration controllability of the platform depends on the decision of where to place actuators. For instance, when the four base joints of Figure 2 are servo-controlled, the positions of every second joints are known. Then, the figure on the righthand-side represents a simplified version of the same system. We can notice that the resulting system does not have any additional mobility. In other words, those four inputs are appropriate to control the position and the shape of the platform. Now, consider Fig. 5 in which three base joints and one second joint of one of the activated serial chains are servo-controlled. The simplified version of this system on the righthand-side does not have any additional mobility. Therefore, those four inputs are also appropriate to control the position and the shape of the platform. Finally, consider Fig. 6 in which the base and the second joints of neighbouring two serial chains are activated. In this case, the resulting simplified version shown on the righthand-side has one additional mobility which might cause an arbitrary, free motion of the platform. Therefore, those four inputs turn out not appropriate to control the position and the shape of the platform.

Besides the locations of the actuator and sensor, we have to consider several aspects in order to successfully execute shape control of the platform of parallel manipulators. They include the shape of the moving platform, the number of chains consisting of the parallel manipulator, and type of joint actuator (prismatic or revolute). Though Figure 2 has just one configuration parameter, the analysis on configuration control will become complicated as the number of the configuration parameters increases. An unified algorithm is needed for general planar systems given in Figure 7 and also this algorithm should be extended to spatial systems operated

Figure 5. Parallel manipulator Having Configuration Controllability

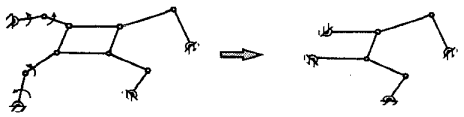

Figure 6. Parallel manipulator Not Having Configuration Controllability

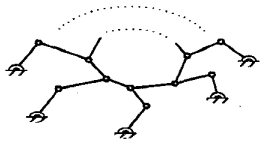

Figure 7. Parallel manipulator Having General Platform Shape

in 3-dimensional space. In this paper, we describe a complete kinematic analysis and design for the planar mechanism given in Fig. 3.

3. Kinematics

3.1 Forward Kinematics

In this section, we describe the forward kinematics of the parallel manipulator given in Fig. 8. We assume that the given manipulator has a parallelogramic platform. The center position (x, y), the orientation angle ϕ of the platform, and the angle α between the link a_1 and the link a_4 or the link a_2 and the link a_3 of the platform are to be controlled. Here, the angle α is denoted as the configuration parameter.

It is commonly known that the forward position solution of general parallel manipulators is not unique. The proposed parallel manipulator is no exception. The position of the platform and the configuration angle cannot be uniquely estimated by using sensor information as many as the number of the mobility. There exists multiple solutions. Several approaches have been reported to obtain a closed-form forward solution of parallel manipulators. Redundant sensors can be used [16] or new parallel manipulators having a closed-form forward solution can be sought [15].

In this section, we discuss how to obtain a unique closed-form forward solution of the proposed system. Firstly, we can obtain a unique closed-form forward solution by replacing the first- and the second-joints or the first- and the third joints of each serial chain by prismatic joints. Merlet [15] mentioned that PPR-type or PRP-type planar manipulators have unique closed-form

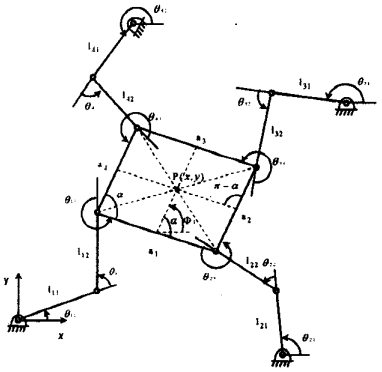

Figure 8. Parallel manipulator with mobility 4

forward solution when placing the sensors at each base joint. The only difference between Merlet's model and ours is that the platform of our system is a parallelogram while Merlet considered a ternary platform. However, the way of obtaining the forward solution is identical. Secondly, consider the case that only revolute joints are employed. However, this case always requires redundant sensors to estimate the forward position. Therefore, we have to decide how many sensors and where to locate those sensors. When placing position sensors at each base joint. Fig. 9 denotes the simplified version of Fig. 8. The resulting system consists of five four-bars with zero mobility in total. In this configuration, once the position solutions for two of the five four-bars are obtained, those of the rest four-bars are easily obtained [15]. Noting that a four-bar has *4th*-order polynomials, 4 different forward position solutions exist. Therefore, one position sensor for each four bar allows closed-loop solution since *2nd*-order polynomial is treated as a closed-loop solution by selecting one of two possible configurations.

3.2 Inverse kinematics

Given the center position (x, y) of the platform, the orientation angle Φ of the platform, and the configuration parameter α, all the joint positions of the parallel chain are obtained. For the first chain, the center position (x, y) of the platform and the orientation angle Φ for each serial chain is, respectively, given as

$$\Phi_1 = \theta_{11} + \theta_{12} + \theta_{13} + \alpha, \tag{2}$$

$$x = l_{11}c_{11} + l_{12}c_{11+12} + \frac{a_1}{2}c_{11+12+13} + \frac{a_4}{2}c_{\Phi}, \tag{3}$$

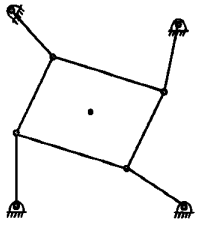

Figure 9. Simplified Version of Figure 8

for the second chain

$$y = l_{11}s_{11} + l_{12}s_{11+12} + \frac{a_1}{2}s_{11+12+13} + \frac{a_4}{2}s_{\Phi}, \tag{4}$$

$$\Phi_2 = \theta_{21} + \theta_{22} + \theta_{23} + \pi - \alpha, \tag{5}$$

$$x = x_{o1} + l_{21}c_{21} + l_{22}c_{21+22} + \frac{a_2c_{21+22+23}}{2} + \frac{a_1c_{\Phi_2}}{2}, \tag{6}$$

$$y = y_{o1} + l_{21}s_{21} + l_{22}s_{21+22} + \frac{a_2s_{21+22+23}}{2} + \frac{a_1s_{\Phi_2}}{2}, \tag{7}$$

for the third chain

$$\Phi_3 = \theta_{31} + \theta_{32} + \theta_{33} + \alpha, \tag{8}$$

$$x = x_{o2} + l_{31}c_{31} + l_{32}c_{31+32} + \frac{a_3}{2}c_{31+32+33} + \frac{a_2}{2}c_{\Phi_3}, \tag{9}$$

$$y = y_{o2} + l_{31}s_{31} + l_{32}s_{31+32} + \frac{a_3}{2}s_{31+32+33} + \frac{a_2}{2}s_{\Phi_3}, \tag{10}$$

and finally for the fourth chain

$$\Phi_4 = \theta_{41} + \theta_{42} + \theta_{43} + \pi - \alpha, \tag{11}$$

$$x = x_{o3} + l_{41}c_{41} + l_{42}c_{41+42} + \frac{a_4}{2}c_{41+42+43} + \frac{a_3}{2}c_{\Phi_4}, \tag{12}$$

$$y = y_{o3} + l_{41}s_{41} + l_{42}s_{41+42} + \frac{a_4}{2}s_{41+42+43} + \frac{a_3}{2}s_{\Phi_4}, \tag{13}$$

where, x_{oi} and y_{oi} $(i=1,2,3)$ denote the positions of the base of each chain with respect to the reference coordinate frame.

The inverse solution for the first chain is obtained as below.

$$\theta_{12} = Atan2(s_{12}, c_{12}), \tag{14}$$

where

$$c_{12} = \frac{x'^2 + y'^2 - l_{11}^2 - l_{12}^2}{2l_1l_{12}}, \quad s_{12} = \sqrt{1 - c_{12}^2}, \tag{15}$$

$$\begin{aligned} x' &= x - \frac{a_1}{2}c_{11+12+13} - \frac{a_4}{2}c_{11+12+13+\alpha}, \\ &= l_{11}c_{11} + l_{12}c_{11+12} \end{aligned} \tag{16}$$

$$\begin{aligned} y' &= x - \frac{a_1}{2}s_{11+12+13} - \frac{a_4}{2}s_{11+12+13+\alpha}, \\ &= l_{11}s_{11} + l_{12}s_{11+12} \end{aligned} \tag{17}$$

and

$$\theta_{11} = Atan2(y, x) - Atan2(k_2, k_1), \tag{18}$$

where

$$k_1 = l_{11} + l_{12}c_{12}, \; k_2 = l_{12}s_{12}. \tag{19}$$

Then,

$$\theta_{13} = \Phi_1 - \alpha - (\theta_{11} + \theta_{12}). \tag{20}$$

Inverse solutions for the rest of chains are obtained the same way.

3.3 First-order Kinematics

The first-order kinematics relates the output velocity vector to the input joint velocity vector. In the following G denotes Jacobian and the left subscript of G denotes the number of serial subchain of the parallel manipulator, the superscript and subscript on the righthand-side of G denote the dependent and independent parameters, respectively. Also, $[G_{\phi}^{u}]_{(*,i)}$ and $[G_{\phi}^{u}]_{(i,*)}$ denote the ith column and the ith row of $[G_{\phi}^{u}]$, respectively. And $[G_{\phi}^{u}]_{(i,j)}$ denotes the (i, j) element of $[G_{\phi}^{u}]$. Then, the velocity relation for the first serial chain is described as

$$\dot{u} = [{}_1G_{\phi}^{u}]_1\dot{\phi}, \tag{21}$$

where

$$\dot{u} = [\dot{x}\ \dot{y}\ \dot{\Phi}]^T,\ {}_1\dot{\phi} = [\dot{\theta}_{11}\ \dot{\theta}_{12}\ \dot{\theta}_{13}\ \dot{\alpha}]^T. \quad (22)$$

Now, augmenting $\dot{\alpha}$ to the above velocity relation, a new output vector $\dot{u}^*$ is defined as

$$\dot{u}^* = \begin{bmatrix} \dot{u} \\ \dot{\alpha} \end{bmatrix}, \quad (23)$$

then the velocity relation for the first chain is described as

$$\dot{u}^* = \begin{bmatrix} [{}_1G_\phi^u] \\ 0\ 0\ 0\ 1 \end{bmatrix} {}_1\dot{\phi} = [{}_1G_a^{u^*}]\,{}_1\dot{\phi}. \quad (24)$$

The same relation can be obtained for the rest of the serial chains. Now, the inverse relation for each chain is denoted as

$${}_i\dot{\phi} = [{}_iG_a^{u^*}]^{-1}\,\dot{u}^*, \quad (25)$$

where we assume that there is no algorithmic singularity in the inversion of the Jacobian $[{}_iG_a^{u^*}]$. Considering the four base joints as the independent joints where actuators and position sensors are placed, the velocity relation relating the output vector to the independent joint vector is constructed by selecting the first row of each inverse-Jacobian of the four serial subchains and forming a matrix relation as below

$$\dot{\phi}_a = \begin{bmatrix} [{}_1G_a^{u^*}]^{-1}_{(1;*)} \\ [{}_2G_a^{u^*}]^{-1}_{(1;*)} \\ [{}_3G_a^{u^*}]^{-1}_{(1;*)} \\ [{}_4G_a^{u^*}]^{-1}_{(1;*)} \end{bmatrix} \dot{u}^*, \quad (26)$$

where

$$\dot{\phi}_a = (\dot{\theta}_{11}\ \dot{\theta}_{21}\ \dot{\theta}_{31}\ \dot{\theta}_{41})^T. \quad (27)$$

Now, inverting the relation of Eq. (26) yields a first-order forward kinematic relation of the system, given by

$$\dot{u}^* = [G_a^{u^*}]\,\dot{\phi}_a, \quad (28)$$

where

$$[G_a^{u^*}] = \begin{bmatrix} [{}_1G_a^{u^*}]^{-1}_{(1;*)} \\ [{}_2G_a^{u^*}]^{-1}_{(1;*)} \\ [{}_3G_a^{u^*}]^{-1}_{(1;*)} \\ [{}_4G_a^{u^*}]^{-1}_{(1;*)} \end{bmatrix}^{-1}. \quad (29)$$

Since there exists a duality between the velocity vector and static force vector, we have

$$T_a = [G_a^{u^*}]^T T_u, \quad (30)$$

where T_u and T_a denote the output force vector and the input joint torque vector, respectively.

4. Kinematic Optimal Design for a Parallel- type Gripping Mechanism

The objective of the kinematic optimization is to design a parallel-type gripping mechanism which can reach the specified workspace, span the given ranges of the specified configuration parameters, and generate a desired force to grasp an object.

4.1 Kinematic Design Indices

4.1.1 Single design index

We consider two kinematic indices ; an isotropic index of the parallel manipulator and a grasping force of the parallel platform. In order to unify the dimension of Jacobian elements, we nondimensionalize the Jacobian elements with respect to the size of the moving platform. Based on the effective force relationship between the operational force vector and the input force vector, the grasping force T_a of the platform is defined from

$$T_a = [G_a^{u^*}]^T_{(*,4)}\,T_a, \quad (31)$$

where $[G_a^{u^*}]^T_{(*,4)}$ denotes the *4th* column of $[G_a^{u^*}]^T$. Now, the ratio of the *2*-norm of the grasping force to that of the input load can be expressed as

$$\frac{\| T_a \|}{\| T_a \|} = \left\{ \frac{T_a{}^T [G_a^{u^*}]_{(*,4)} [G_a^{u^*}]^T_{(*,4)} T_a}{T_a{}^T T_a} \right\}^{\frac{1}{2}} = p, \quad (32)$$

where the scalar p is given as

$$p = \{ [G_a^{u^*}]_{(*,4)} [G_a^{u^*}]^T_{(*,4)} \}^{\frac{1}{2}}. \quad (33)$$

Then, the 2-norm of the grasping force is defined as

$$\| T_a \| = p \cdot \| T_a \|. \quad (34)$$

The global maximum grasping force is defined with respect to the entire workspace of the manipulator as

$$\Sigma_F = \frac{\int_W \| T_a \|\, dW}{\int_W dW}, \quad (35)$$

where the workspace of manipulators is denoted as

$$W = \int_W dW. \quad (36)$$

Also, a manipulator should be designed so that it has well-conditioned workspace which allows its end-effector to move from one regular value to another without passing through a critical value (singularity). An isotropic index is a criterion to measure such phenomenon. In order to measure the motion isotropic characteristic of the system, the first-order kinematic property for the center position (x, y) of the platform and the orientation angle Φ of the platform should be analyzed. For this, a sub-Jacobian $[G_a^u]$ except the last row of $[G_a^{u^*}]$ is considered. Then, the isotropic index σ_I is defined as

$$\sigma_I = \frac{\sigma_{\min}}{\sigma_{\max}}, \quad (37)$$

where $\sigma_{\min}$ and $\sigma_{\max}$ denote the minimum and maximum singular value of $[G_a^u]$, respectively. The global isotropic index is defined with respect to the entire workspace of the manipulator as

$$\Sigma_I = \frac{\int_W \sigma_I\, dW}{W}. \quad (38)$$

The design of a manipulator system can be based on any particular criterion. However, the single criterion-based design does not provide sufficient control on the range of the design parameters involved. Therefore, multi-criteria based design has been proposed [5]. However, the previous multi-criteria methods did not provide any systematic design procedure and flexibility in design. To consider these facts, a composite design index is proposed in the following section.

4.1.2 Composite design index

In order to cope with multi-criteria based design, we employ a concept of kinematic composite design index.

Various design indices introduced above are usually incommensurate concepts due to differences in unit and physical meanings, and therefore should not be combined with normalization and weighting functions unless they are transferred into a common domain. As an initial step to this process, preferential information should be given to each design parameter and each design index. Then, each design index is transferred to common preference design domain which ranges from zero to one. Here, the preference given to each design criterion is very subjective to the designer. Preference can be given to each criterion by weighting. This provides flexibility in design. For both $\| T_a \|$ and σ_I, the best preference is given the minimum value, and the least preference is given the minimum value of the criterion. Then, the design index is transferred into common preference design domain as below

$$\tilde{\Sigma}_I = \frac{\Sigma_I - \Sigma_{I\min}}{\Sigma_{I\max} - \Sigma_{I\min}}, \tag{39}$$

where '~' implies that the index is transferred into the common preference design domain. Note that each composite design index is constructed such that a large value represents a better design. Large $\tilde{\Sigma}_I$ implies that the system possesses good isotropic characteristic within the given workspace, and also large $\tilde{\Sigma}_F$ implies that the system produces large grasping force for an unit actuator load within the given workspace.

A set of optimal design parameters is obtained based on max-min principle. Initially the minimum values among the design indices for all set of design parameters are obtained, and then a set of design parameters, which has the maximum of the minimum values, is chosen as the optimal set of design parameters. Based on this principle, the composite global design index(*CGDI*) is defined as the minimum value of the above mentioned design indices at a set of design parameters, and given as

$$CGDI = \min\{ \tilde{\Sigma}_I^{\beta}, \tilde{\Sigma}_F^{\gamma} \}. \tag{40}$$

The upper Greek letters (β, γ, etc) represent the degree of weighting, and usually large value implies large weighting. In general, the value of weighting is determined based on fuzzy measure such as normal, very, more or less, absolutely and so on. Though those fuzzy measures can be defuzzified as crisp values very subjectively, the following cases have been employed; normal is equivalent to 1, very is equivalent to 2, more or less is equivalent to 0.5, absolutely is equivalent to ∞, and so on. [17] In order to evenly satisfy the several design objectives for all design indices, all of the weighting factors are set to 1.0. Now, a set of optimal design parameters is chosen as the set that has the maximum *CGDI* among all *CGDI*'s calculated for all set of design parameters.

4.2 Optimization Methodology

To deal with a nonlinear optimization with constrains, three numerical methods are used. The exterior penalty function method is employed to transform the constrained optimization problem into an unconstrained optimal problem. Powell's method is applied to obtain an optimal solution for the unconstrained problem, and quadratic interpolation method is utilized for uni-directional minimization [18].

The link lengths and the base location of each serial subchain, and the dimensions of the platform of the parallel manipulator can be cited as kinematic design parameters. Assume that the four serial subchains have a symmetric configuration. In other words, the first and second link lengths of the four serial chains are identical, respectively. Therefore, two design parameters exist for serial chains. The platform is an equilateral parallelogram. Therefore, it has one design parameters(a). The proposed gripper mechanism will be attached at the end of a macro-manipulator providing global motion. Therefore, we plan to place the four base locations of the four serial-chains around the end-position of a macro-manipulator symmetrically. For the base location of the parallel manipulator, only one design parameter (r : radius of the base platform) exists when the four base locations are placed symmetrically. In total, there exists five design parameters in the design of the proposed parallel manipulator.

Initially, we define the desired workspace and the range of the configuration parameter of the proposed parallel manipulator. Since this device is to be utilized as a micro-positioning device after grasping, the workspace will be smaller than the macro-manipulator. Here, the workspace will be given the inside area of a square centered at the middle of the workspace. The size of the workspace will be proportional to that of the platform. It is given as

$$-0.25r \le \Delta x,\ \Delta y \le 0.25r, \tag{41}$$

where Δx, Δy denote the distances from the center of the workspace in the $x-$ and $y-$direction, respectively. The range of orientation of the platform is given as

$$-10^o \le \phi \le 10^o, \tag{42}$$

and the range of the configuration parameter will be given as

$$90^o - \eta \le a \le 90^o + \eta, \tag{43}$$

where the angle η will be set as 30^o.

Now, kinematic constraints associated with the five design parameters are given as

$$0.01m \le l_{a1},\ l_{a2},\ a \le 0.10m,$$
$$0.01m \le r \le 0.05\ or\ 0.10m. \tag{44}$$

We consider three different platform sizes since the platform size is decided according to the size of object to be grasped. Kinematic optimization for the proposed parallel manipulator has been performed for the case of $\beta = 1$, $\gamma = 1$, for the case of $\beta = 3$, $\gamma = 1$ in which large weighting is given the grasping force, and for the case of $\beta = 1$, $\gamma = 3$ in which large weighting is given the isotropic index. The optimal design parameters obtained from the optimization is given in Table 1 which denotes the case for $r_{\max} = 0.05m$, while Table 2 denotes the case for $r_{\max} = 0.10m$. In general, better kinematic characteristics are observed for large base platform which, however, results in larger link size as compared to those of the smaller base platform. For $r_{\max} = 0.05m$, Figure 10 and 11 illustrate the optimized configurations for Case I and Case II, respectively. In general, the smaller the platform size is, the larger the base size is, and vice versa.

To compare the results, we plot the grasping force and

the isotropic index for Case I with $r_{max} = 0.05m$. We can observe from Figs. 12 through 14 that overall trends of the two indices follow the given design objectives. Note that a trade-off exists between the isotropic characteristic and the grasping force. Based on the simulation result, we could conclude that the proposed parallelogramic gripping mechanism can be designed either for creating large grasping force or possessing good motion isotropy.

The proposed parallel manipulator can also be employed as a good micro-positioning device in that it has enough degree-of-freeedom(3), has light weight allowing high bandwidth, and possesses enough positioning and sensing capabilities which are operational requirements necessary for micro-positioning devices[19,20].

5. Conclusions

Currently employed robot gripper has a simple geometry which is often not appropriate to grasp an object having irregular shape or large volume. We proposed a parallel mechanism which is able to grasp any object having irregular shape or large volume by folding the parallelogramic platform, and also it can be utilized as a micro-positioning device after grasping.

Though we considered a simple example having one configuration parameter, an unified algorithm should be derived for general planar systems given in Figure 7 and also this algorithm should be extended to spatial systems operated in the 3-dimensional space. Currently, we are developing the proposed device for grasping experiment.

Appendix

The components of $[{}_1G_\phi^u]$ are given in the following :

$$[{}_1G_\phi^u]_{(1,1)} = -y, \quad \text{(A1)}$$

$$[{}_1G_\phi^u]_{(1,2)} = -(y - l_{11}s_{11}), \quad \text{(A2)}$$

$$[{}_1G_\phi^u]_{(1,3)} = -(y - l_1 s_{11} - l_{12}s_{11+12}), \quad \text{(A3)}$$

$$[{}_1G_\phi^u]_{(1,4)} = -(\frac{a_4}{2} s_{11+12+13+a}), \quad \text{(A4)}$$

$$[{}_1G_\phi^u]_{(2,1)} = -x, \quad \text{(A5)}$$

$$[{}_1G_\phi^u]_{(2,2)} = -(x - l_1 c_{11}), \quad \text{(A6)}$$

$$[{}_1G_\phi^u]_{(2,3)} = -(x - l_{11}c_{11} - l_{12}c_{11+12}), \quad \text{(A7)}$$

$$[{}_1G_\phi^u]_{(2,4)} = -(\frac{a_4}{2} c_{11+12+13+a}), \quad \text{(A8)}$$

and

$$[{}_1G_\phi^u]_{(3,i)} = 1, \quad (i = 1-4). \quad \text{(A9)}$$

References

[1] Colbaugh, R. Seraji, H., and Glass, K., "Obstacle Avoidance for Redundant Robots Using Configuration Control," *J. of Robotic Systems* Vol. 6, pp. 72-744 1989.

[2] Burdick, J.W., "On the Inverse Kinematics of Redundant Manipulators : Characterization of the Self-Motion Manifolds," *IEEE International Conference on Robotics and Automation* pp. 264-270 1989.

[3] Erdman, A.G. and Sandor, G.N., Mechanical Design: Analysis and Synthesis, *Vol.1, 2nd ed. Prentice Hall* 1991.

[4] Freeman, R.A. and Tesar, D., "Dynamic Modeling of Serial and Parallel Mechanisms/Robotic Systems," 1988 *ASME Biennial Mechanism Conf.* Kissimmee FL. DE-Vol. 15-2, pp. 7-21 1988.

[5] Hayward, V. and Kurtz, R., "Multi-Criteria Design of a Parallel Wrist Mechanism with Actuator Redundancy," *IEEE Trans. on Journal of Robotics and Automation* Vol. 8, No. 5, pp. 644-651 1992.

[6] Kumar, V.J. and Gardner, J., "Kinematics of Redundantly Actuated Closed Chains," IEEE *Journal of Robotics and Auto.* Vol. 6, No. 2, pp. 269-273 1990.

[7] Meyer, A.N. and Angeles J., "Force Optimization in Redundantly Actuated Closed-Chain Kinematic Chains," *IEEE Int. Conf. on Robotics and Automation* Scottsdale AZ. Vol. 1, pp. 951-956 1989.

[8] Ropponen, T. and Nakamura, Y., "Singularity-Free Parameterization and Performance Analysis of Actuation Redundancy," *Proc. IEEE Int. Conf. on Robotics and Automation* Cioncinnati OH. pp. 806-811 1990.

[9] Walker, I.D., Freeman, R.A., and Marcus, S.I., "Cooperating Robot Manipulators," *Proc. IEEE Int. Conf. on Robotics and Automation,* Vol. 1, pp. 606-611 1989.

[10] Kang, H.J., Yi, B.J., Cho, W., and Freeman, R.A., "Constraint Embedding Approaches for General Closed-Chain System Dynamics in Terms of a Minimum Coordinate Set," *1990 ASME Biennial Mechanism Conf.* DE-Vol. 24 pp. 126-132 1990.

[11] Yi, B.J., Oh, S-R., Suh, I.H., and You, B.J., "Synthesis of Frequency Modulator via Redundant Actuation : The Case for a Five-bar Finger Mechanism," *IEEE International Conference on Intelligent Robots and Systems(IROS)* Sept. 1997.

[12] Kim, W.K., Lee, J.Y., and Yi, B.J., "RCC Characteristics of Planar-Spherical 3 Degree-of-Freedom Parallel Mechanisms with Joint Compliances," *IEEE/RSJ International Conference on Intelligent Robots and Systems(IROS)* pp. 360-367 Nov. 1996.

[13] Yi, B.J., Suh, I.H., Oh, S.-R., "Analysis of A 5-bar Finger Mechanism Having Redundant Actuators With Applications to Stiffness and Frequency Modulations" *IEEE Int. Conf. on Robotics and Aut.* pp.759-765 1 1997.

[14] Kim, Whee-Kuk, Lee, Jun-Yong , and Yi, Byung-Ju, "Analysis for A Planner 3 Degree-of-Freedom Parallel Mechanism With Activity Adjustable Stiffness Characteristics" *IEEE International Conference on Robotics and Automation* pp. 2663-2670 1997.

[15] Merlet, "Direct Kinematics of Planar Parallel Manipulator," *IEEE International Conference on Robotics and Automation* pp. 3744-3750 April 1996.

[16] Han, K., Chung, W.K., and Youm, Y., "Local Structurization for the Forward Kinematics of Parallel Manipulators Using Extra Sensor Data," *IEEE Int. Conf. on Robotics and Automation* pp. 541-520 1995.

[17] Terano, T., Asai, K., and Sugeno, M., Fuzzy Systems and Its Applications, 1st ed., *Hardourt Brace Jovanovitch Publishers* San Diego 1993.

[18] Arora, J.S., "Introduction to Optimal Design," *McGraw Hill* 1989.

[19] Yamagata, Y. and Higuchi, T., "A Micropositioning Device for Precision Automatic Assembly Using Impact Force of Piezoelectric Elements," *IEEE Int. Conference on Robotics and Automation* pp. 666-671 April 1995.

[20] Hudgens, J.C., "Modeling and Analysis of A Fully-Parallel Six Degree-of-Freedom Micromanipulator." Master Thesis, Department of Mechanical Eng., The University of Texas at Austin 1986.

Table 1. Optimization Results for $r_{max} = 0.05m$

Platform length (m)	ISO:GF	Average Σ_I (ISO)	Average Σ_F (GF)	Link1 length (m)	Link2 length (m)	Base radius (m)
Case I 0.02	1 : 1	0.44	8.64	0.05	0.05	0.05
	3 : 1	0.55	6.98	0.06	0.05	0.05
	1 : 3	0.39	9.60	0.07	0.06	0.05
Case II 0.04	1 : 1	0.22	3.86	0.03	0.03	0.01
	3 : 1	0.37	1.76	0.02	0.02	0.01
	1 : 3	0.12	6.86	0.04	0.04	0.01
Case III 0.08	1 : 1	0.28	4.51	0.07	0.07	0.01
	3 : 1	0.47	2.12	0.08	0.07	0.01
	1 : 3	0.16	7.35	0.08	0.08	0.01

Table 2. Optimization Results for $r_{max} = 0.10m$

Platform length (m)	ISO:GF	Average Σ_I (ISO)	Average Σ_F (GF)	Link1 length (m)	Link2 length (m)	Base radius (m)
Case I 0.02	1 : 1	0.57	10.41	0.1	0.09	0.08
Case II 0.04	1 : 1	0.46	7.81	0.1	0.09	0.09
Case III 0.08	1 : 1	0.28	4.51	0.07	0.07	0.01

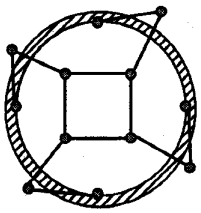

Figure 10. Optimized Configuration for Case I

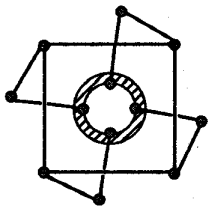

Figure 11. Optimized Configuration for Case II

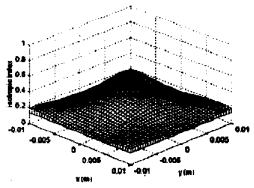

(a) Isotropic index

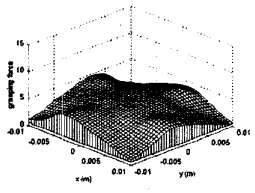

(b) Grasping Force

Figure 12. Kinematic Indices for Case I(ISO:GF=1:1)

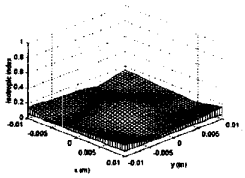

(a) Isotropic index

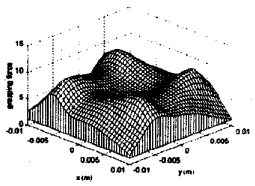

(b) Grasping Force

Figure 13. Kinematic Indices for Case I(ISO:GF=1:3)

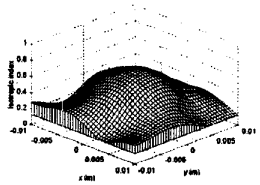

(a) Isotropic index

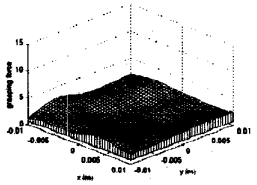

(b) Grasping Force

Figure 14. Kinematic Indices for Case I(ISO:GF=3:1)